**Cell Death and Differentiation (2016) 23,** 1727–1736
 1350-9047/16
www.nature.com/cdd

# Caspase-2 deficiency accelerates chemically induced liver cancer in mice

**S Shalini[1], A Nikolic[1], CH Wilson[1], J Puccini[1], N Sladojevic[1], J Finnie[2], L Dorstyn[1] and S Kumar*[,1]**

**Aberrant cell death/survival has a critical role in the development of hepatocellular carcinoma (HCC). Caspase-2, a cell death protease, limits oxidative stress and chromosomal instability. To study its role in reactive oxygen species (ROS) and DNA damage-induced liver cancer, we assessed diethylnitrosamine (DEN)-mediated tumour development in caspase-2-deficient (*Casp2*$^{-/-}$) mice. Following DEN injection in young animals, tumour development was monitored for 10 months. We found that DEN-treated *Casp2*$^{-/-}$ mice have dramatically elevated tumour burden and accelerated tumour progression with increased incidence of HCC, accompanied by higher oxidative damage and inflammation. Furthermore, following acute DEN injection, liver injury, DNA damage, inflammatory cytokine release and hepatocyte proliferation were enhanced in mice lacking caspase-2. Our study demonstrates for the first time that caspase-2 limits the progression of tumourigenesis induced by an ROS producing and DNA damaging reagent. Our findings suggest that after initial DEN-induced DNA damage, caspase-2 may remove aberrant cells to limit liver damage and disease progression. We propose that *Casp2*$^{-/-}$ mice, which are more susceptible to genomic instability, are limited in their ability to respond to DNA damage and thus carry more damaged cells resulting in accelerated tumourigenesis.**
*Cell Death and Differentiation* (2016) **23,** 1727–1736; doi:10.1038/cdd.2016.81; published online 12 August 2016

The initiator caspase, caspase-2, has recently emerged as a tumour suppressor with loss of this protein being associated with increased lymphomagenesis in *ATM*-deficient mice and *Eμ-Myc* transgenic mice, and *MMTV/c-neu*-driven mammary carcinoma.[1–4] Caspase-2 has been shown to protect cells from oxidative stress, DNA damage and genomic instability, and caspase-2 deficiency is linked to chromosomal instability and aneuploidy.[1,5,6] However, currently little is known about the possible role of caspase-2 in carcinogenesis induced by ROS and DNA damage.

Hepatocellular carcinoma (HCC) is among the most common cancers and is the second leading cause of cancer-related deaths worldwide.[7] Development of HCC is multifaceted progressing from DNA damage to dysplasia, adenoma development and malignant transformation of hepatocytes.[7,8] The major risk factors of HCC include viral hepatitis, excessive alcohol consumption, carcinogens and metabolic diseases.[7,8] Despite this, the molecular causes of the disease are relatively less understood. Diethylnitrosamine (DEN) is a DNA alkylating and ROS inducing carcinogen that is widely used as a model to study the progression of HCC in rodents.[9,10] DEN treatment mimics the human disease by inducing DNA damage in proliferating hepatocytes of infant mice.[9] Increases in the generation of ROS and accumulation of DNA damage can stimulate an inflammatory response and hyperproliferation that helps drive tumour progression.[7–10] It has increasingly been recognised that apoptosis and compensatory proliferation are crucial for progression of certain cancers including HCC.[11–13] While loss of apoptosis would indirectly favour proliferation, this is not universally true, for example loss of PUMA, or hepatocyte-specific deletion of Bid, impedes HCC by preventing compensatory proliferation.[14–20]

Metabolic state is another important regulator of HCC progression and there is increasing evidence that caspase-2 has a subtle role in regulating this process.[21,22] Caspase-2 deficiency in mice results in metabolic perturbations and aged caspase-2 mice show increased oxidative stress and DNA damage.[5,21,23] DEN-induced tumour formation involves the generation of DNA adducts,[10] and human HCC is commonly associated with genomic instability.[24] These observations, combined with the known tumour suppressor role in lymphoma and MMTV-driven mammary carcinoma, suggest a possible role of caspase-2 in HCC. Thus, we sought to explore whether caspase-2 deficiency would promote chemically induced hepatic carcinogenesis in liver. We observed that DEN-induced liver tumours in *Casp2*$^{-/-}$ mice were consistently larger and more advanced than those in WT mice, providing the first evidence that caspase-2 deficiency has a role in ROS and DNA damaged mediated HCC.

## Results

**Caspase-2 deficiency causes increased incidence of HCC.** *Casp2*$^{-/-}$ mice injected with DEN at 15 days old consistently showed enlarged livers with increased tumour burden compared with WT mice at 10 months post injection

[1]Centre for Cancer Biology, University of South Australia, Adelaide, SA 5000, Australia and [2]SA Pathology and School of Medical and Veterinary Science, University of Adelaide, Adelaide, SA 5000, Australia
*Corresponding author: S Kumar, Centre for Cancer Biology, University of South Australia, Frome Road, Adelaide, SA 5000, Australia. Tel: +61 882223738; Fax: +61 882223162; E-mail: sharad.kumar@unisa.edu.au
**Abbreviations:** HCC, hepatocellular carcinoma; DEN, diethylnitrosamine; ROS, reactive oxygen species; ALT, alanine aminotransferase; AST, aspartate transaminase; LDH, lactate dehydrogenase; ALP, alkaline phosphatase; TUNEL, terminal deoxynucleotidyl transferase dUTP nick end labelling; PCNA, proliferating cell nuclear antigen; HMGB1, high-mobility group box 1
Received 11.1.16; revised 05.6.16; accepted 07.7.16; Edited by G Melino; published online 12.8.2016

(Figures 1a and c). While all *Casp2*$^{-/-}$ mice injected with DEN formed tumours at 10 months, 2/11 DEN-injected WT mice were tumour free (Figure 1b). Histological analysis of livers from young (6–9 weeks) non-DEN-injected tumour free *Casp2*$^{-/-}$ mice had no abnormal liver morphology or perturbed hepatocyte nuclei. However, consistent with previous findings[23] by 10 months of age all PBS-injected *Casp2*$^{-/-}$ mice displayed an increase in nuclear volume (karyomegaly) and binucleation (Supplementary Figure 1a and b).

In DEN-injected WT mice, livers were usually macroscopically normal with occasional protrusion of tumour nodules (Figure 1a). Microscopically, altered hepatic foci were often present (Supplementary Figure 1c). Foci were composed of hepatocytes generally resembling those found in adjacent unaffected hepatic parenchyma, but with a cytoplasmic tinctorial appearance ranging from eosinophilic, basophilic, clear or vacuolated (fatty change). Hepatocytes in tumour masses were generally well differentiated and resembled the tinctorial span found in hepatic foci. Mitoses were rare to absent. Tumour masses were usually well circumscribed, but frequently compressed the surrounding parenchyma, and were designated hepatocellular adenomas (HCAs) (Figure 1d and Supplementary Figure 1c).

Macroscopicaly, livers of *Casp2*$^{-/-}$ mice often showed multiple tumour masses of varying size and colour (Figure 1a). Microscopically, these contained many hepatocytes with enlarged, hyperchromatic, atypical nuclei of round to ovoid, more elliptical, or sometimes lobulated, appearance, sometimes bi- or multinucleated, and often showed prominent nucleoli (Figure 1d and Supplementary Figure 1d–f). Mitotic figures were usually common and some were abnormal (Supplementary Figure 1e). These tumours were diagnosed as HCCs. Some of these neoplasms contained hepatocytes with numerous eosinophilic cytoplasmic inclusions (globular bodies) of varying size, which have been correlated with a reduced proliferation index (Supplementary Figure 1d). No metastasis was observed in any mice. We used Glypican 3 as a marker for HCC[7] and observed positive staining in 5/7 DEN-injected *Casp2*$^{-/-}$ mice livers while none of the WT mice showed any positive reaction (Figure 1d).

**Increased oxidative stress, liver damage and inflammation in *Casp2*$^{-/-}$ mice.** DEN generates ROS and causes DNA damage, which contributes to the development of HCC.[9,24] As *Casp2*$^{-/-}$ mice are more susceptible to oxidative stress-induced damage to lipids, DNA and protein,[24,25] these parameters were measured in liver (Figures 2a, b and d). While no difference in lipid peroxidation (MDA) was observed between WT and *Casp2*$^{-/-}$ DEN-injected mice (Figure 2a), protein carbonylation (Figure 2d) and 8-OHdG levels (Figure 2b) were significantly higher in DEN-injected *Casp2*$^{-/-}$ mice, indicating greater oxidative protein and DNA damage. SOD activity increased in both groups after DEN injections but was significantly lower in the *Casp2*$^{-/-}$ mice (Figure 2c). Serum analysis revealed elevation of liver function enzymes ALT and ALP in DEN-injected *Casp2*$^{-/-}$ mice compared with WT (Figures 2e and f), indicating increased liver damage. While cholesterol, HDL and LDL increased following DEN injection, no difference was observed between WT and *Casp2*$^{-/-}$ mice (Supplementary Figure 2). Along with increased liver damage, IL6 levels were increased in DEN-injected mice and were significantly elevated in DEN-injected *Casp2*$^{-/-}$ mice compared with WT (Figure 2g). Increases in IL1$\alpha$ and IL1$\beta$ levels were also observed in DEN-injected *Casp2*$^{-/-}$ mice compared with WT (Figures 2h and i).

Liver damage and inflammation is often accompanied by increases in hepatic cell death and proliferation.[13] We used immunoblot analysis and TUNEL to determine levels of apoptosis in DEN-injected mice. Slightly increased cleavage of caspase-3 was observed by immunoblotting in DEN-injected WT, but not in *Casp2*$^{-/-}$ mice (Figure 3a). However, there was no difference in PARP cleavage or levels of PUMA (Figure 3a) or in the frequency of TUNEL-positive cells (Figure 3b). In addition, no difference in cleaved caspase-3 was detected by immunohistochemical analysis of liver sections (Supplementary Figure 3). Proliferation of hepatocytes as assessed by PCNA staining of DEN-injected livers was high in both WT and *Casp2*$^{-/-}$ mice, but no difference was observed between genotypes (Figure 3c).

**Altered metabolism and stress-response pathways in advanced stage *Casp2*$^{-/-}$ tumours.** We next investigated the contribution of altered metabolism and stress/DNA damage response pathways to the increased susceptibility of DEN-induced HCC in *Casp2*$^{-/-}$ mice. Activation of stress-response pathways was analysed by immunoblotting with an increase in phospho-JNK being observed in *Casp2*$^{-/-}$ mice along with a trend towards increased ERK activation (Figure 4 and Supplementary Figure 4).

Previous studies have reported altered metabolic profile in *Casp2*$^{-/-}$ mice.[19] During the development of HCC and HCA, the activity of several enzymes involved in glycogen metabolism, oxidative pentose phosphate pathway and glycolysis is different.[25] It is known that adenomas largely contain basophilic cells with high fat or glycogen content.[25] In addition, G-6-Pase and ALPase activity increases as adenomas develop into carcinomas while G6PDH activity declines in carcinomas.[25] DEN injection did not alter the levels of glycogen or G-6-P in WT or *Casp2*$^{-/-}$ mice (Figures 5a and b). However, compared with WT, glycogen levels were lower in both PBS- and DEN-injected *Casp2*$^{-/-}$ mice and G-6-P was lower in DEN-injected *Casp2*$^{-/-}$ mice (Figures 5a and b). In addition, G6PDH activity was reduced in DEN-injected compared with PBS-injected *Casp2*$^{-/-}$ mice (Figure 5c). Another group of proteins that regulate metabolism and have been linked with DEN-induced HCC is Sirtuins.[26–28] We therefore measured Sirt1 and 3 expression and activity. Sirt1 activity was reduced in DEN-treated *Casp2*$^{-/-}$ mice, but not in WT (Figure 5d), whereas Sirt3 activity was significantly increased by DEN in WT mice but not in *Casp2*$^{-/-}$ mice (Figure 5e). Surprisingly, an increase in total Sirt1 protein levels was detected in DEN-treated *Casp2*$^{-/-}$ mice (Figure 5f). This may be a compensatory response from the decrease in Sirt1 activity. No differences in total Sirt3 protein levels were observed (Figure 5f). P53 is frequently inactivated (mutated) in HCC, impairing the DNA damage response.[24] Therefore, we investigated p53 and p21 levels by immunoblotting. Total p53 protein levels were somewhat increased in DEN-treated WT

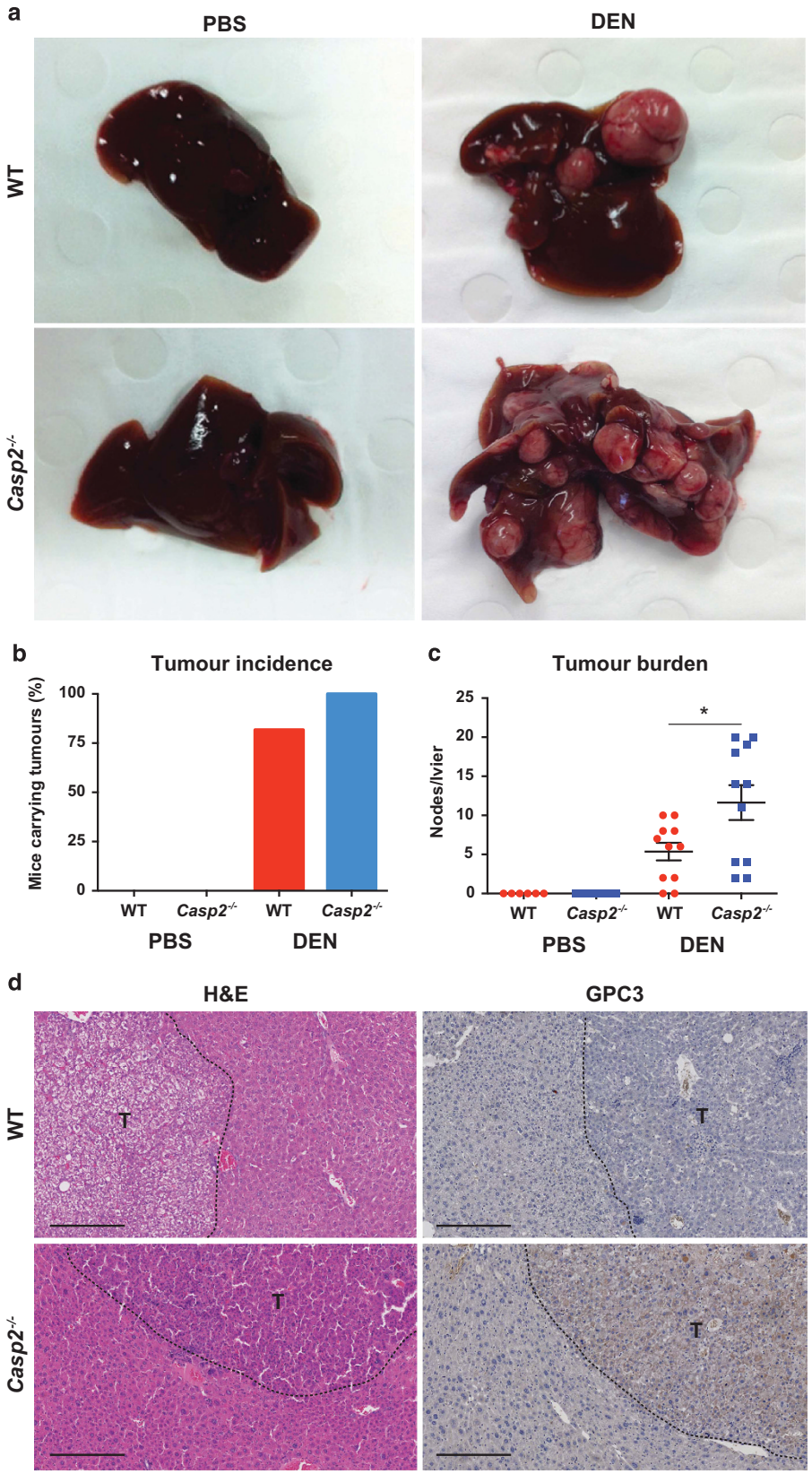


**Figure 1** Loss of caspase-2 accelerates HCC development. (**a**) Macroscopic view of representative images of mice liver, 10 months after PBS/DEN administration. (**b**) Tumour incidence and (**c**) tumour burden in DEN-injected mice. Values are given as mean ± S.E.M. ($n = 6$, PBS and $n = 11$, DEN). Statistics were performed using Student's *t*-test: $^*P < 0.05$. (**d**) Representative haematoxylin and eosin-stained images of mice liver tumours and immunohistochemical staining for Glypican 3, as a marker of HCC showing positive in *Casp2*$^{-/-}$ mice, 10 months after PBS/DEN administration. Scale bar represents 250 $\mu$m. Tumour nodes outlined and labelled as 'T'

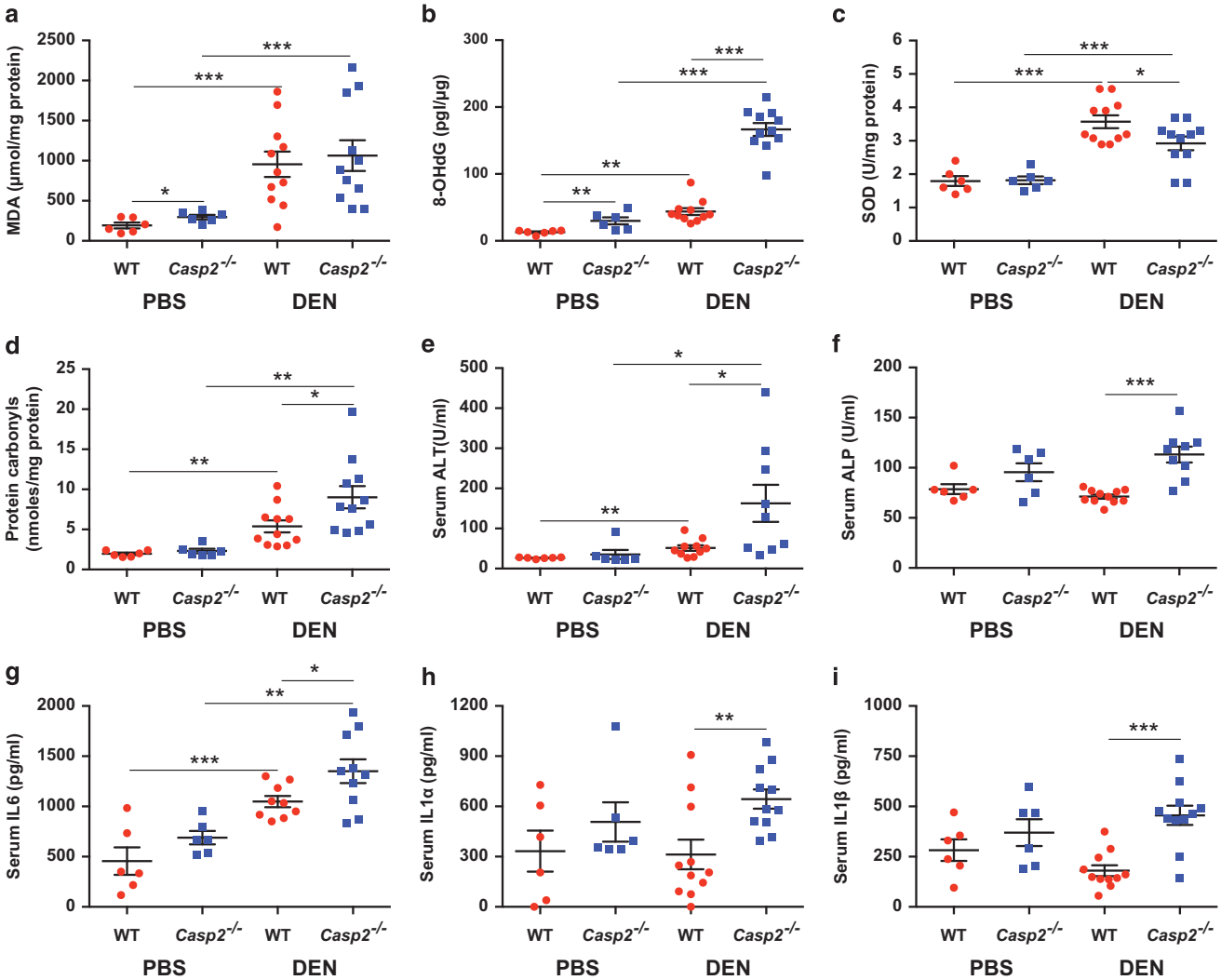


**Figure 2** *Casp2*$^{-/-}$ mice have higher oxidative damage and inflammation. (**a**) Lipid peroxidation, (**b**) oxidatively modified DNA; 8-OHdG, (**c**) SOD (total) activity and (**d**) protein carbonyls were determined in mice liver lysates. (**e**) Alanine transaminase (ALT), (**f**) Alkaline phosphatase (ALP), (**g**) IL6, (**h**) IL1$\alpha$ and (**i**) IL1$\beta$ were measured in serum. Values are given as mean ± S.E.M. ($n=6$, PBS and $n=11$, DEN). Statistics were performed using Student's *t*-test. *$P<0.05$, **$P<0.01$ and ***$P<0.001$

mice and were significantly higher in DEN-treated *Casp2*$^{-/-}$ mice compared with WT as were p21 levels.

**Increased cellular damage in the absence of cell death is responsible for proliferative advantage in *Casp2*$^{-/-}$ mice.** To further investigate the mechanisms that lead to increased tumour incidence and burden in *Casp2*$^{-/-}$ mice, we carried out short-term DEN exposure. After 24 h DEN, little to no TUNEL-positive cells were observed in *Casp2*$^{-/-}$ mice liver compared with WT but at 48 h both WT and *Casp2*$^{-/-}$ mice displayed TUNEL-positive hepatocytes with no difference between genotypes (Figure 6a). Damage was localised to the central canal regions. γH2Ax is a well-known marker for dsDNA breaks and 48 h after DEN injection, γH2Ax was increased in both WT and *Casp2*$^{-/-}$ mice, with *Casp2*$^{-/-}$ mice having significantly higher number of γH2Ax-positive cells compared with WT (Figure 6b). Notably, although reduced TUNEL reactivity was observed at 24 h in *Casp2*$^{-/-}$ mice, pale necrotic centrolobular region was evident in both WT and *Casp2*$^{-/-}$ mice (Supplementary Figure 5). PCNA staining was then performed on the same sections. At 48 h post DEN injection, there were significantly more PCNA-positive cells in the *Casp2*$^{-/-}$ mice compared with WT mice (Figure 6c). To assess the extent of liver damage, we measured serum ALT and observed increased activity in *Casp2*$^{-/-}$ mice at 48 h (Figure 6d). Compared with WT, IL6 levels were increased in *Casp2*$^{-/-}$ mice at 24 and 48 h and IL1$\alpha$ levels at 48 h after DEN injection (Figures 6g and e). Furthermore, IL1$\alpha$ and IL1$\beta$ were further increased in DEN-injected *Casp2*$^{-/-}$ mice at 48 h compared with 24 h (Figures 6e and f).

**Increased DNA damage in adult *Casp2*$^{-/-}$ mice treated with DEN.** In additional experiments, the effect of DEN was also studied by injecting 25 mg/kg DEN in 6-week-old mice. Mice were maintained for 1 year and then analysed for tumour development. None of the mice formed tumours. This

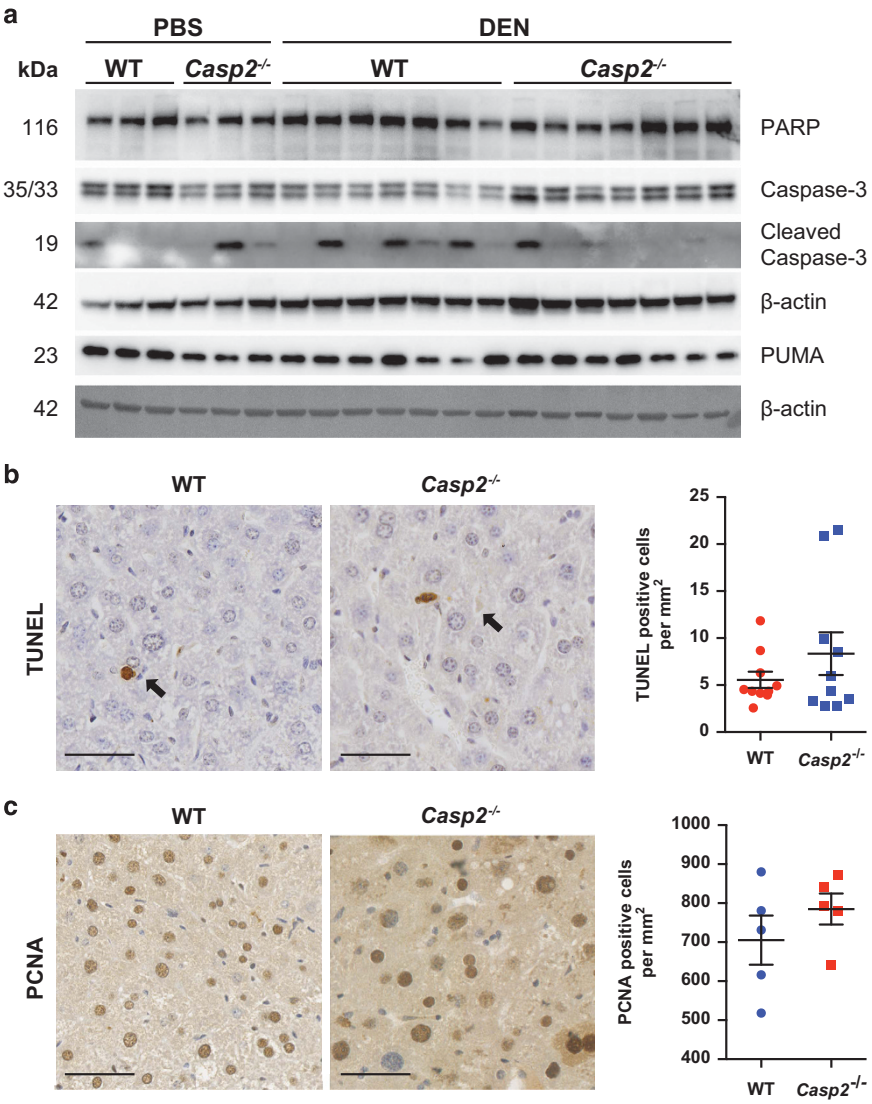


**Figure 3** *Casp2*$^{-/-}$ mice display no difference in cell death or proliferation. (**a**) Representative western blots showing increased caspase-3 cleavage in DEN-injected WT mice. (**b**) Representative images of TUNEL-positive cells in mice liver 10 months after PBS/DEN administration. Scale bar represents 50 $\mu$m. (**c**) Immunohistochemical staining for PCNA, as a marker of cell proliferation showing high frequency of PCNA-positive hepatocytes in brown, 10 months following DEN exposure. Scale bar represents 50 $\mu$m

is consistent with the fact that a single DEN dose produces tumours when injected in infant mice when hepatocytes are proliferating. Consistent with previous findings,[23] *Casp2*$^{-/-}$ mice showed significant karyomegaly, increased anisocytosis, presence of intranuclear vacuoles and bi/multinucleate cells, suggesting severe DNA damage and dysregulated cell cycling (Supplementary Figure 7a). TNF$\alpha$ and IL6 were also significantly higher in DEN-injected *Casp2*$^{-/-}$ mice (Supplementary Figure 7b and c). Consistent with mice injected at 15 days, an increase in ERK and JNK activation was also observed in DEN-injected *Casp2*$^{-/-}$ livers (Supplementary Figure 7d).

## Discussion

In this study, we provide a direct evidence for caspase-2 in delaying DEN initiated liver tumours. We find higher DNA damage in *Casp2*$^{-/-}$ mice when exposed to DEN compared with WT mice. *Casp2*$^{-/-}$ mice also had increased liver damage and formed aggressive HCCs.

Hepatocarcinogenesis is a multistep process that can be caused by a number of agents that ultimately lead to malignant transformation of hepatocytes.[7–10,29] HCC induction by DEN is a commonly utilised mouse model.[9,10] DEN is an alkylating agent that induces DNA damage by reacting with nucleophiles such as DNA bases.[9,10] Furthermore, DEN bioactivation involves the activity of P450 enzymes which produces ROS and results in oxidative stress.[9,30] ROS-induced DNA, protein and lipid damage is known to contribute to hepatocarcinogenesis.[30–32] Single DEN dose causes HCC in 80–100% rodents in about 45–105 weeks[33] with the sequential emergence of preneoplastic hepatic foci, HCAs and then HCC.[25] *Casp2*$^{-/-}$ mice formed carcinomas after 10 months of DEN injections while the majority of tumours in

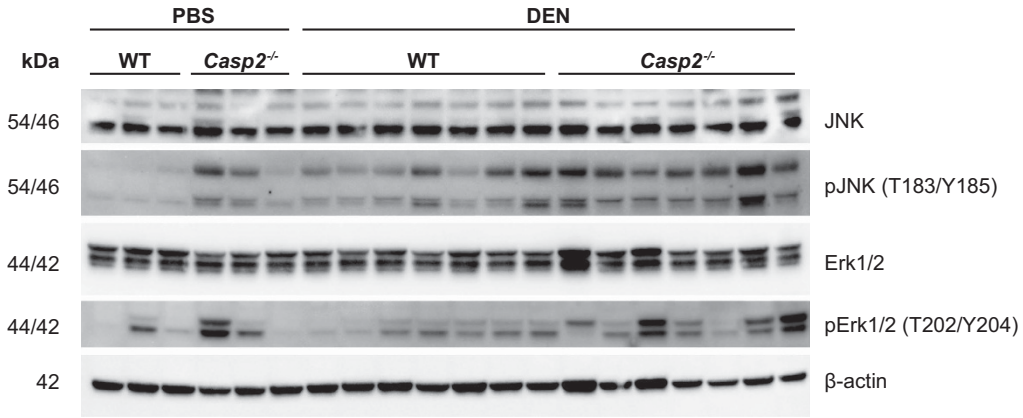


**Figure 4** *Casp2*$^{-/-}$ mice display stress-induced JNK activation. Immunoblot analysis of MAPK activation pathway. Activation of the JNK stress-response pathway was significantly increased in *Casp2*$^{-/-}$ mice. There was also a trend towards ERK pathway activation

WT mice were classified as adenomas, suggesting that tumours in *Casp2*$^{-/-}$ mice were more advanced.

One reason for the advanced tumorigenic state may be higher ROS levels in *Casp2*$^{-/-}$ mice leading to increased oxidative stress-induced DNA damage. We have shown earlier that *Casp2*$^{-/-}$ mice experience excessive oxidative stress with ageing and oxidative stress response[5,23] and here again show increased susceptibility to more oxidative DNA and protein damage after DEN injection. Sirtuins contribute to the response to oxidative stress and the lower Sirt1 and Sirt3 activities in DEN-injected *Casp2*$^{-/-}$ mice may in part contribute to increased susceptibility to DEN-induced damage. Sirt3 has several substrates involved in oxidative stress response such as MnSOD.[34] Consistent with the lack of increased Sirt3 activity as observed in WT, SOD activity was lower in DEN-injected *Casp2*$^{-/-}$ mice, which is likely to contribute to higher oxidative damage in this group. Further, higher serum ALT levels and ALP levels indicate increased liver injury in this group of mice.

A number of signalling pathways have been implicated in DEN-induced liver carcinogenesis, and stress activated JNK expression was higher in *Casp2*$^{-/-}$ mice. JNK activation leads to upregulation of several proapoptotic genes such as TNF$\alpha$.[35] A dual role for JNK in development of HCC has been proposed.[36] In hepatocytes, higher JNK activity prevents HCC development while JNK activation in non-parenchymal liver cells promotes HCC development.[36] p53 is a well-known tumour suppressor that also regulates the DNA damage response.[37] DEN-injected WT mice showed a significant upregulation of total p53 protein and *p53* expression (Supplementary Figure 6b). On the other hand, *mdm2* was reduced in DEN-injected *Casp2*$^{-/-}$ mice (Supplementary Figure 6c). As mdm2 is a target of p53,[38] reduced gene expression in *Casp2*$^{-/-}$ mice may be a consequence of failure of p53 activation in this group. Our immunoblot data indicated increased p53 and p21 protein levels in DEN-injected *Casp2*$^{-/-}$ mice. While no change in protein levels of PUMA, another p53 target that mediates DNA damage was observed, following DEN treatment control *Casp2*$^{-/-}$ mice had elevated *puma* gene expression (Supplementary Figure 6d), which correlates with the observations that DNA damage is already higher in ageing *Casp2*$^{-/-}$ mice.[22] Levels of *noxa*, another proapoptotic BH3-only protein, remained unchanged (Supplementary Figure 6e).

Interestingly, we also observed that IL1$\alpha$, IL1$\beta$ and IL6 levels were higher in DEN-injected *Casp2*$^{-/-}$ mice. Inflammation has a key role in various types of cancers.[39,40] The classical liver inflammatory cytokines described in a number of HCC-linked liver inflammation models include IL6, TNF-$\alpha$, IL1$\alpha$ and IL1$\beta$.[40,41] Several studies have reported higher IL6 levels in cases of HCC.[42,43] DEN exposure promotes production of IL6 in Kupffer cells and stimulates tumour growth. Male mice have higher IL6 levels compared with females due to oestrogen-mediated inhibition reflecting the lower incidence of DEN-induced HCC in females[44] and its importance in HCC progression can be realised from the fact that after ablation of IL6 male mice do not produce any more HCC than female mice.[43,45]

Previous studies have demonstrated that in two different models of DNA damage-driven mouse tumours, deficiency of caspase-2 had no significant effect. The authors found that lymphomagenesis in mice induced by repeated exposure to low-dose $\gamma$-irradiation, or formation of fibrosarcoma by injection of 3-methylcholanthrene (3-MC), a carcinogen forming bulky adducts with DNA, were similar in WT and *Casp2*$^{-/-}$ mice.[46] These data suggested that tumour suppression by caspase-2 is not involved in DNA damage-induced tumourigenesis. Our data on the other hand suggest that caspase-2 is a strong suppressor of DEN-induced HCC. Although it remains unclear why suppressor effects of caspase-2 are so vastly different in these models of tumourigenesis, it is possible that different mechanisms of tumourigenesis (HCC *versus* lymphomagenesis and fibrosarcoma) contribute to differences in DNA damage response. For example, in addition to DNA damage, increased inflammatory and compensatory proliferation responses also have important roles in HCC, but may have limited roles in $\gamma$-irradiation-induced lymphomagenesis and 3-MC-dependent fibrosarcoma formation. Further studies will be required to fully understand the tumour suppressive effects of caspase-2 in

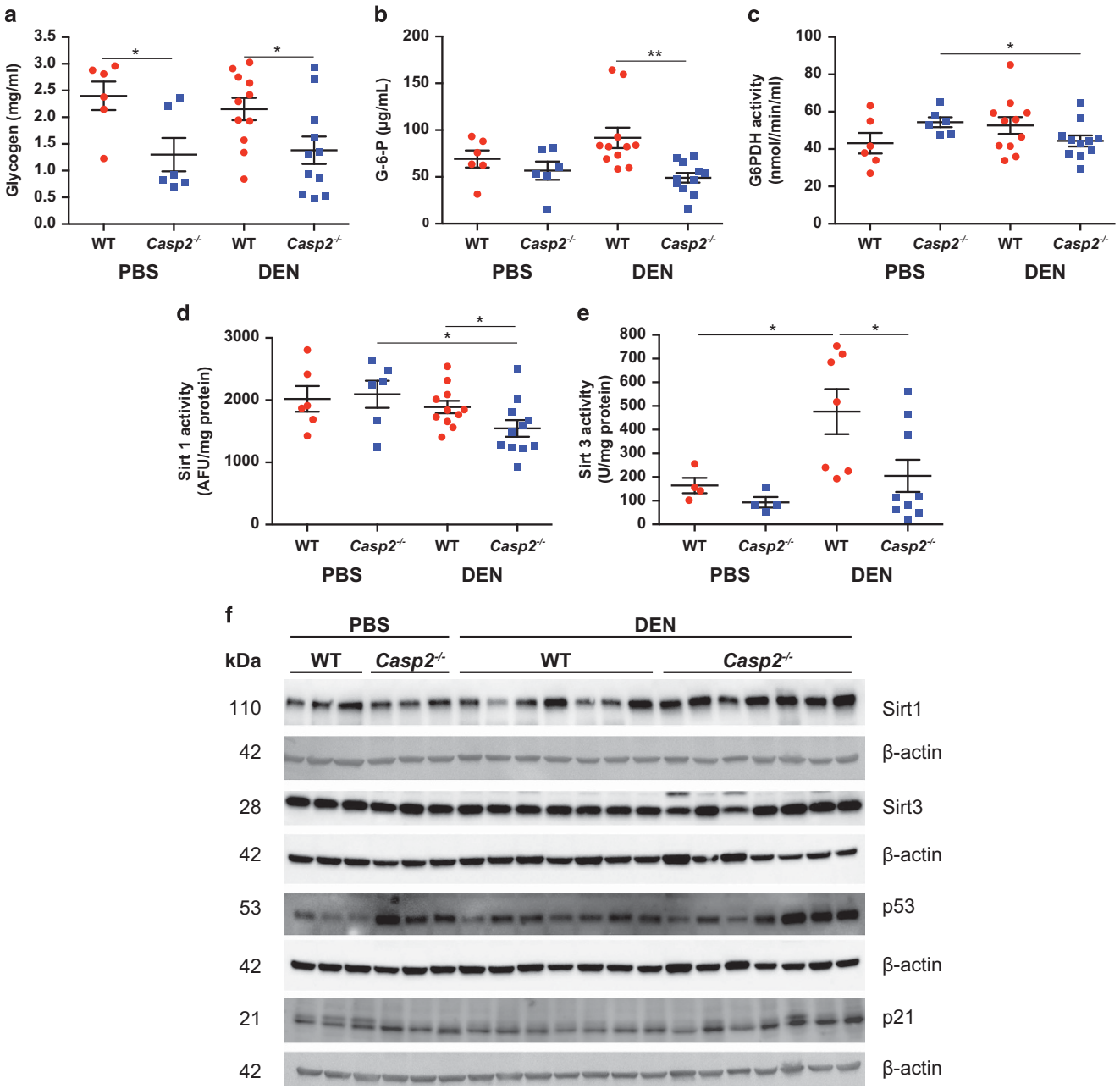


**Figure 5** Metabolic state of *Casp2*$^{-/-}$ mice favours tumour progression. Reduced (**a**) glycogen levels, (**b**) glucose-6-phosphate levels and (**c**) G6PDH activity in DEN-injected *Casp2*$^{-/-}$ mice. Decrease in Sirt1 (**d**) and Sirt3 (**e**) activities in DEN-injected *Casp2*$^{-/-}$ mice liver 10 months after PBS/DEN administration. Values are given as mean ± S.E.M. ($n=6$, PBS and $n=11$, DEN). Statistics were performed using Student's *t*-test: $^{*}P<0.05$ and $^{**}P<0.01$. (**f**) Immunoblot analysis showing increased Sirt1 protein expression in DEN-injected *Casp2*$^{-/-}$ mice. Upregulation of p53 and its downstream effector p21 was also observed

HCC and whether caspase-2 acts in more than one pathway in hepatocytes to limit DEN-induced carcinogenesis.

## Materials and Methods

**Mice.** Male WT and *Casp2*$^{-/-}$ mice on a C57BL/6J background[47] were used for all experimental studies. All animals were maintained in specific pathogen-free conditions in a 12-h/12-h light/dark cycle and treated in accordance with protocols approved by the SA Pathology/Central Northern Adelaide Health Services Animal Ethics Committee. To induce liver cancer, 15-day-old male pups were injected i.p. with 25 mg/kg bodyweight DEN (Sigma-Aldrich, St. Louis, MO, USA) and controls were injected with PBS. Mice were kept for 10 months after which they were humanely killed and blood and tissues collected. Acute effects of DEN were assessed in 6- to 7-week-old male mice injected i.p. with 100 mg/kg bodyweight DEN. Mice were humanely killed and tissues collected 24 and 48 h post injection.

**Serum analysis and ELISA.** Liver function tests (ALT, AST, LDH, ALP activity), triglycerides, cholesterol, HDL and LDL were determined in the serum by automated analysis (SA Pathology, Adelaide, SA, Australia). IL6 was measured in mice serum using the mouse IL6 ELISA kit (eBioscience Inc., San Diego, CA, USA), TNF$\alpha$, IL1$\alpha$ and IL1$\beta$ were measured using commercially available mouse DuoSet ELISA kits (R&D Systems, Minneapolis, MN, USA).

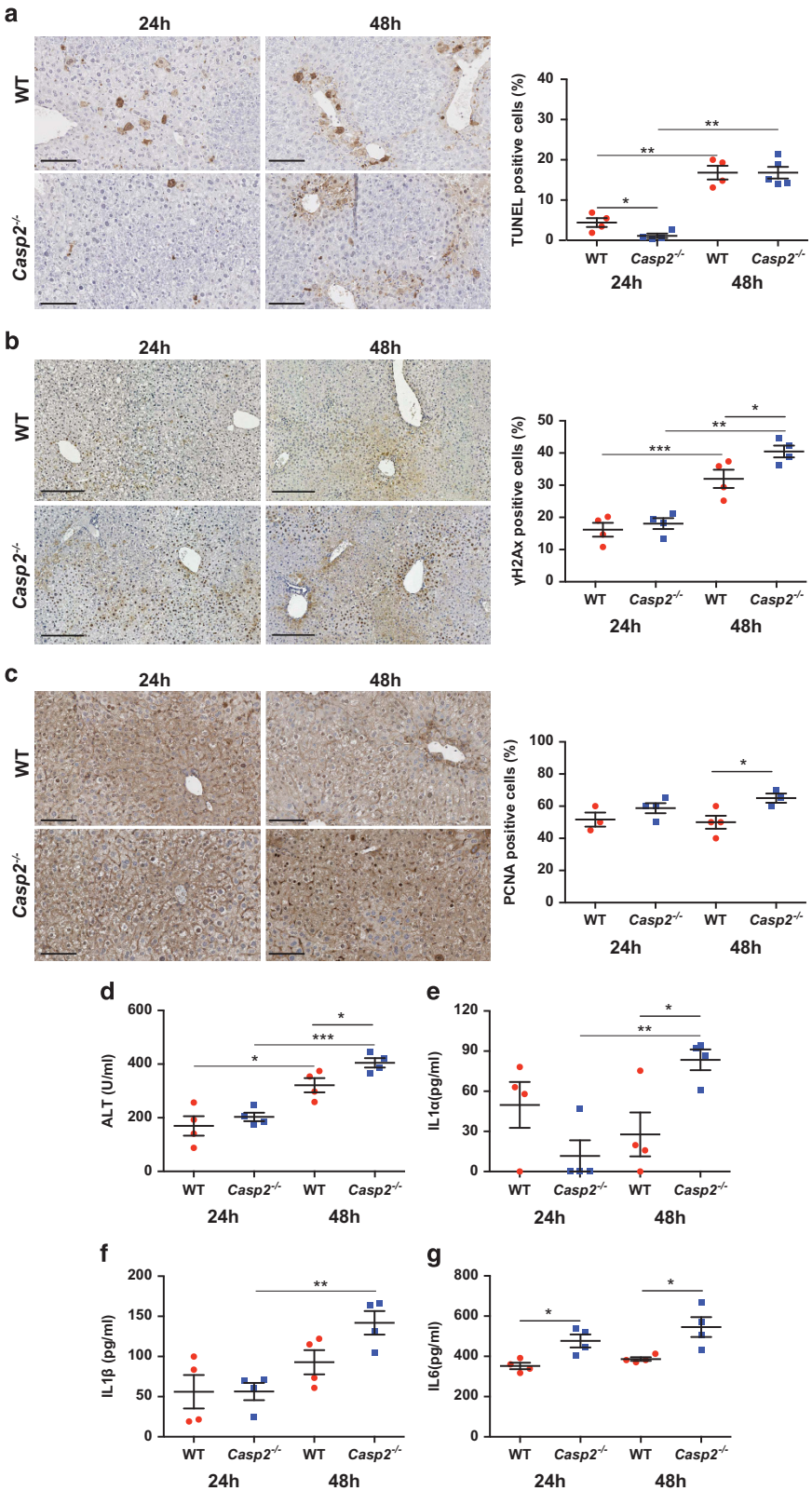
a
24h
48h
WT
Casp2-/-
TUNEL positive cells (%)
WT
Casp2-/-
WT
Casp2-/-
24h
48h
b
24h
48h
WT
Casp2-/-
γH2Ax positive cells (%)
WT
Casp2-/-
WT
Casp2-/-
24h
48h
c
24h
48h
WT
Casp2-/-
PCNA positive cells (%)
WT
Casp2-/-
WT
Casp2-/-
24h
48h
d
ALT (U/ml)
WT
Casp2-/-
WT
Casp2-/-
24h
48h
e
IL1α(pg/ml)
WT
Casp2-/-
WT
Casp2-/-
24h
48h
f
IL1β (pg/ml)
WT
Casp2-/-
WT
Casp2-/-
24h
48h
g
IL6(pg/ml)
WT
Casp2-/-
WT
Casp2-/-
24h
48h

**Figure 6** Acute response to DEN-induced liver damage in *Casp2*$^{-/-}$ mice. (**a**) Representative images of cell death (TUNEL) 24 and 48 h after 100 mg/kg bodyweight DEN injection in 6- to 7-week-old mice. TUNEL-positive hepatocytes were few initially at 24 h, but increased at 48 h and comparable between the two groups as quantitated on the right. Scale bar represents 100 $\mu$m. (**b**) Immunohistochemical localisation for $\gamma$H2Ax. Higher frequency of positive hepatocytes was observed in *Casp2*$^{-/-}$ mice 48 h after acute DEN treatment. Scale bar represents 250 $\mu$m. (**c**) Immunohistochemical staining for PCNA and quantitation of PCNA-positive cells (right) showed a significant increase in proliferating cell number in *Casp2*$^{-/-}$ mice 48 h after DEN exposure. Scale bar represents 100 $\mu$m. Increased serum (**d**) ALT, (**e**) IL1$\alpha$, (**f**) IL1$\beta$ and (**g**) IL6 after 48 h DEN injection. Data are shown as mean $\pm$ S.E.M. ($n=4$). Statistics were performed using Student's *t*-test: *$P<0.05$, **$P<0.01$ and ***$P<0.001$

**Measurement of oxidative damage to protein, lipids and DNA.** Protein, lipid and DNA oxidation was quantified using commercially available Protein Carbonyl Colorimetric Assay, TBARS Assay and 8-OHdG E1A Kits (Cayman Chemical, Ann Arbour, MI, USA) according to the manufacturer's instructions.

**Measurement of liver metabolites and Sirt1 and Sirt3 activities.** Glucose-6-phosphate, glycogen and glucose-6-phosphate dehydrogenase activities were measured in liver tissue homogenates using commercially available assay kits (Sigma; BioVision, Milpitas, CA, USA). Sirt1 and Sirt3 enzymatic activities were measured in liver tissue homogenates using the commercially available SIRT1 Fluorometric Kit (Enzo Life Sciences, Plymouth Meeting, PA, USA) and SIRT3 Direct Fluorescent Screening Assay Kit (Cayman Chemical, Ann Arbour, MI, USA) according to the manufacturer's instructions.

**Histology and TUNEL.** Liver tissue was fixed in 10% formalin for 24 h, embedded in paraffin, sectioned (7 $\mu$m) and stained with haematoxylin and eosin. Detection of apoptotic cells by TUNEL was performed on formalin-fixed, paraffin-embedded liver sections using the ApopTag Peroxidase In Situ Apoptosis Detection kit (Millipore, Billerica, MA, USA) according to the manufacturer's instructions. Digital images were acquired by using a NanoZoomer (Hamamatsu Photonics, Hamamatsu City, Shizuoka Pref., Japan).

**Immunohistochemistry.** For immunohistochemical localisation studies, formalin-fixed, paraffin-embedded liver sections were deparaffinised in xylene and rehydrated in graded ethanol series. Endogenous peroxidase activity was blocked with 3% (vol/vol) $H_2O_2$/PBS solution. Antigen retrieval was performed by sub-boiling the sections for 10 min in 0.1 M Citrate Buffer Antigen Retrieval Solution (pH 6.0). Non-specific antibody binding was blocked using and 5% (vol/vol) FBS/PBS solution with Tween-20 for 30 min. Tissue sections were incubated with anti-cleaved caspase-3 (9664; Cell Signaling Technology, Beverly, MA, USA) diluted 1:200, anti-glypican3 (ab66596; Abcam, Cambridge, MA, USA) diluted 1:200, anti-PCNA (clone PC10; Cell Signaling Technology) diluted 1:250 and anti-phospho histone $\gamma$H2AX (Ser139) (Cell Signaling) primary antibody diluted 1:100 in blocking solution overnight at 4 °C. Tissue sections were sequentially incubated with anti-mouse or anti-rabbit biotinylated secondary antibody diluted 1:250 in blocking solution (GE Healthcare, Waukesha, WI, USA) and Avidin/Biotin Complex reagent (VectaStain ABC kit, Vector Labs, Burlingame, CA, USA) at room temperature. Peroxidase substrate (3,3′-diaminobenzidine) was added for colour development, followed by counterstaining with Mayer's haematoxylin solution (Sigma-Aldrich). Tissue sections were then dehydrated in graded ethanol series and coverslips mounted by using DePex mounting media (Sigma-Aldrich). Cells with positive staining were scored in at least five fields of view and reported as mean $\pm$ S.E.M. Three or more mice were used in each group.

**Immunoblotting.** Liver tissues were homogenised in RIPA lysis buffer containing 50 mM Tris-HCl (pH 7.4), 150 mM NaCl, 2 mM EGTA, 2 mM EDTA, 25 mM sodium fluoride, 25 mM $\beta$-glycerophosphate, 0.1 mM sodium orthovanadate, 0.1 mM PMSF, 0.2% Triton X-100, 0.3% Nonidet P-40 and protease inhibitors (Roche Diagnostics, Basel, Switzerland) and phosphatase inhibitors (Thermo Fisher Scientific, Rockford, IL, USA). Homogenates were further treated by three freeze/thawed cycles in liquid nitrogen, clarified by centrifugation at 16 000 $\times$ *g* and protein concentration determined by the BCA quantification (Pierce, Thermo Fisher Scientific). In all, 40 $\mu$g of lysates was resolved by SDS-PAGE, transferred onto PVDF membrane and probed for the specified antibody for 2 h at room temperature or overnight at 4 °C. Secondary antibodies, conjugated with alkaline phosphatase (AP; Millipore), horse-radish peroxidase (HRP; GE Healthcare, Waukesha, WI, USA) or Cy5 (GE Healthcare), were incubated at room temperature for 1 h. Proteins were visualised using ECF (Amersham, Little Chalfont, UK) or enhanced chemiluminescence (SuperSignal West Femto Maximum Sensitivity Substrate; Thermo Fisher Scientific). Membranes were immuno-blotted with the following antibodies: p44/42 MAPK (Erk1/2) (137F5), phospho-p44/42 MAPK (Erk1/2) (Thr202/Tyr204) (D13.14.4E), JNK (2C6), phospho-SAPK/JNK (Thr183/Tyr185) (81E11), cleaved caspase-3 (9664), caspase-3 (8G10), p53 (IC12), Sirt1 (2028), Sirt3 (D22A3), GAPDH (14C10) (Cell Signalling Technology, Beverly, MA, USA), p21 (clone SX118, BD Biosciences, Franklin Lakes, NJ, USA), caspase-2 (clone 11B4; Millipore), $\beta$-actin (AC15; Sigma-Aldrich) and PUMA (ab9643) (Abcam).

**Quantitative PCR analysis.** Total RNA was isolated from MEFs using TRIzol reagent (Invitrogen, Carlsbad, CA, USA) and cDNA synthesised using oligo-dT primers and High Capacity cDNA reverse transcription kit (Applied Biosciences, Foster City, CA, USA). Real-time PCR was performed on a Rotor-Gene 6000 (Qiagen, Valencia, CA, USA) using RT2 Real-Time SYBR Green/ROX PCR Master Mix (Qiagen) as per the manufacturer's instructions. The following primer sets were used for the amplification of mouse genes in qPCRs: *β-catenin;* 5′-CACCACAGCTCCTTCCCTGA-3′, 5′- CATTGCATACTGCCCGTCAA-3′, *mdm2;* 5′-GAAGGAGCACAGGAAAATATATGCA-3′, 5′-GTCTGCTCTCACTCAGCGATGT-3′, *Trp53;* 5′-CTCACTCCAGCTACCTGAAGA-3′, 5′-AGAGGCAGTCAGTCAGTCTGAGTCA-3′; *puma;* 5′-ATGCCTGCCTCACCTTCATCT-3′, 5′-AGCACAGGATTCACAGTCTGGA-3′; *noxa;* 5′-ACTGTGGTTCTGGCGCAGAT-3′, 5′-TTGAGCACACTCGTCCTTCAA-3′, *HGPRT;* 5′-GAGAGCGTTGGGCTTACCTC-3′, 5′-CTAATCACGACGCTGGGACT-3′.

Reactions were performed in triplicate and the mRNA expression levels normalised against the internal control gene *HGPRT* using the $2^{-\Delta\Delta CT}$ method.

**Statistical analysis of data.** Statistical analysis was performed using GraphPad Prism software (v 6.0, San Diego, CA, USA). Data are expressed as mean $\pm$ S.D. or mean $\pm$ S.E.M. Statistical significance was calculated with a Student's *t*-test. $P<0.05$ was considered to be significant.

## Conflict of Interest

The authors declare no conflict of interest.

**Acknowledgements**. We thank Alyshea Collaco for injecting mice and the staff at the SA Pathology animal resource facility for maintaining the mouse strains. This work was supported by the National Health and Medical Research Council (NHMRC) of Australia project grant (1021456), a Cancer Council Collaborative Research Fellowship to LD, an NHMRC Early Career Research Fellowship to CW (1073771) and NHMRC Senior Principal Research Fellowships (1002863 and 1103006) to SK.

### Author contributions

SS, LD and SK conceptualised and designed the study; SS, AN, JP, CW and NS performed experiments; SS, AN, LD, CW and SK analysed the data; JF helped with tumour histopathology analyses; SS, CW and SK wrote and revised the paper. All authors commented on the manuscript drafts and edited the text.

1. Puccini J, Dorstyn L, Kumar S. Caspase-2 as a tumour suppressor. *Cell Death Differ* 2013; **20**: 1133–1139.
2. Puccini J, Shalini S, Voss AK, Gatei M, Wilson CH, Hiwase DK *et al.* Loss of caspase-2 augments lymphomagenesis and enhances genomic instability in Atm-deficient mice. *Proc Natl Acad Sci USA* 2013; **110**: 19920–19925.
3. Ho LH, Taylor R, Dorstyn L, Cakouros D, Bouillet P, Kumar S. A tumor suppressor function for caspase-2. *Proc Natl Acad Sci USA* 2009; **106**: 5336–5341.
4. Parsons MJ, McCormick L, Janke L, Howard A, Bouchier-Hayes L, Green DR. Genetic deletion of caspase-2 accelerates MMTV/c-neu-driven mammary carcinogenesis in mice. *Cell Death Differ* 2013; **20**: 1174–1182.
5. Shalini S, Puccini J, Wilson CH, Finnie J, Dorstyn L, Kumar S. Caspase-2 protects against oxidative stress in vivo. *Oncogene* 2015; **34**: 4995–5002.
6. Dorstyn L, Puccini J, Wilson CH, Shalini S, Nicola M, Moore S *et al.* Caspase-2 deficiency promotes aberrant DNA-damage response and genetic instability. *Cell Death Differ* 2012; **19**: 1288–1298.

7. Kim JU, Shariff MIF, Crossey MME, Gomez-Romero M, Taylor-Robinson SD. Hepatocellular carcinoma: Review of disease and tumor biomarkers. *World J Hepatol* 2016; **8**: 471–484.
8. Tang ZY. Hepatocellular carcinoma–cause, treatment and metastasis. *World J Gastroenterol* 2001; **7**: 445–454.
9. Vesselinovitch SD, Koka M, Mihailovich N, Rao KV. Carcinogenicity of diethylnitrosamine in newborn, infant, and adult mice. *J Cancer Res Clin Oncol* 1984; **108**: 60–65.
10. Verna L, Whysner J, Williams GM. N-nitrosodiethylamine mechanistic data and risk assessment: bioactivation, DNA-adduct formation, mutagenicity, and tumor initiation. *Pharmacol Ther* 1996; **71**: 57–81.
11. Maeda S, Kamata H, Luo JL, Leffert H, Karin M. IKKbeta couples hepatocyte death to cytokine-driven compensatory proliferation that promotes chemical hepatocarcinogenesis. *Cell* 2005; **121**: 977–990.
12. Wei JC, Meng FD, Qu K, Wang ZX, Wu QF, Zhang LQ *et al.* Sorafenib inhibits proliferation and invasion of human hepatocellular carcinoma cells via up-regulation of p53 and suppressing FoxM1. *Acta Pharmacol Sin* 2015; **36**: 241–251.
13. Buitrago-Molina LE, Marhenke S, Longerich T, Sharma AD, Boukouris AE, Geffers R *et al.* The degree of liver injury determines the role of p21 in liver regeneration and hepatocarcinogenesis in mice. *Hepatology* 2013; **58**: 1143–1152.
14. Wree A, Johnson CD, Font-Burgada J, Eguchi A, Povero D, Karin M *et al.* Hepatocyte-specific Bid depletion reduces tumor development by suppressing inflammation-related compensatory proliferation. *Cell Death Differ* 2015; **22**: 1985–1994.
15. Qiu W, Wang X, Leibowtiz B, Yang W, Zhang L, Yu J. PUMA-mediated apoptosis drives chemical hepatocarcinogenesis in mice. *Hepatology* 2011; **54**: 1249–1258.
16. Teoh N, Pyakurel P, Dan YY, Swisshelm K, Hou J, Mitchell C *et al.* Induction of p53 renders ATM-deficient mice refractory to hepatocarcinogenesis. *Gastroenterology* 2010; **138**: 1155–1165, e1151–e1152.
17. Liedtke C, Zschemisch NH, Cohrs A, Roskams T, Borlak J, Manns MP *et al.* Silencing of caspase-8 in murine hepatocellular carcinomas is mediated via methylation of an essential promoter element. *Gastroenterology* 2005; **129**: 1602–1615.
18. Bai L, Ni HM, Chen X, DiFrancesca D, Yin XM. Deletion of Bid impedes cell proliferation and hepatic carcinogenesis. *Am J Pathol* 2005; **166**: 1523–1532.
19. Weber A, Boger R, Vick B, Urbanik T, Haybaeck J, Zoller S *et al.* Hepatocyte-specific deletion of the antiapoptotic protein myeloid cell leukemia-1 triggers proliferation and hepatocarcinogenesis in mice. *Hepatology* 2010; **51**: 1226–1236.
20. Pierce RH, Vail ME, Ralph L, Campbell JS, Fausto N. Bcl-2 expression inhibits liver carcinogenesis and delays the development of proliferating foci. *Am J Pathol* 2002; **160**: 1555–1560.
21. Wilson CH, Shalini S, Filipovska A, Richman TR, Davies S, Martin SD *et al.* Age-related proteostasis and metabolic alterations in Caspase-2-deficient mice. *Cell Death Dis* 2015; **6**: e1597.
22. Shalini S, Dorstyn L, Dawar S, Kumar S. Old, new and emerging functions of caspases. *Cell Death Differ* 2015; **22**: 526–539.
23. Shalini S, Dorstyn L, Wilson C, Puccini J, Ho L, Kumar S. Impaired antioxidant defence and accumulation of oxidative stress in caspase-2-deficient mice. *Cell Death Differ* 2012; **19**: 1370–1380.
24. Yang S, Chang C, Wei R, Shiue Y, Wang S, Yeh Y. Involvement of DNA damage response pathways in hepatocellular carcinoma. *Bio Med Res Int* 2014; **;2014**: 153867.
25. Hacker HJ, Mtiro H, Bannasch P, Vesselinovitch SD. Histochemical profile of mouse hepatocellular adenomas and carcinomas induced by a single dose of diethylnitrosamine. *Cancer Res* 1991; **51**: 1952–1958.
26. Schug TT, Li X. Sirtuin 1 in lipid metabolism and obesity. *Ann Med* 2011; **43**: 198–211.
27. Garcia-Rodriguez JL, Barbier-Torres L, Fernandez-Alvarez S, Gutierrez-de Juan V, Monte MJ, Halilbasic E *et al.* SIRT1 controls liver regeneration by regulating bile acid metabolism through farnesoid X receptor and mammalian target of rapamycin signaling. *Hepatology* 2014; **59**: 1972–1983.
28. Zhang YY, Zhou LM. Sirt3 inhibits hepatocellular carcinoma cell growth through reducing Mdm2-mediated p53 degradation. *Biochem Biophys Res Commun* 2012; **423**: 26–31.
29. Farber E. Liver cell cancer: insights into the pathogenesis of hepatocellular carcinoma in humans from experimental hepatocarcinogenesis in the rat. *Monogr Pathol* 1987; **28**: 199–222.
30. Kolaja KL, Klaunig JE. Vitamin E modulation of hepatic focal lesion growth in mice. *Toxicol Appl Pharmacol* 1997; **143**: 380–387.
31. Valko M, Rhodes CJ, Moncol J, Izakovic M, Mazur M. Free radicals, metals and antioxidants in oxidative stress-induced cancer. *Chem Biol Interact* 2006; **160**: 1–40.
32. Kawanishi S, Hiraku Y, Murata M, Oikawa S. The role of metals in site-specific DNA damage with reference to carcinogenesis. *Free Radic Biol Med* 2002; **32**: 822–832.
33. Heindryckx F, Colle I, Van Vlierberghe H. Experimental mouse models for hepatocellular carcinoma research. *Int J Exp Pathol* 2009; **90**: 367–386.
34. Tao R, Coleman MC, Pennington JD, Ozden O, Park SH, Jiang H *et al.* Sirt3-mediated deacetylation of evolutionarily conserved lysine 122 regulates MnSOD activity in response to stress. *Mol Cell* 2010; **40**: 893–904.
35. Dhanasekaran DN, Reddy EP. JNK signaling in apoptosis. *Oncogene* 2008; **27**: 6245–6251.
36. Das M, Garlick DS, Greiner DL, Davis RJ. The role of JNK in the development of hepatocellular carcinoma. *Genes Dev* 2011; **25**: 634–645.
37. Meek DW. Tumour suppression by p53: a role for the DNA damage response? *Nat Rev Cancer* 2009; **9**: 714–723.
38. Wu X, Bayle JH, Olson D, Levine AJ. The p53-mdm-2 autoregulatory feedback loop. *Genes Dev* 1993; **7**: 1126–1132.
39. deVisser KE, Coussens LM. The inflammatory tumor microenvironment and its impact on cancer development. *Contrib Microbiol* 2006; **13**: 118–137.
40. Mantovani A, Allavena P, Sica A, Balkwill F. Cancer-related inflammation. *Nature* 2008; **454**: 436–444.
41. Grivennikov SI, Greten FR, Karin M. Immunity, inflammation, and cancer. *Cell* 2010; **140**: 883–899.
42. Grivennikov SI, Karin M. Dangerous liaisons: STAT3 and NF-kappaB collaboration and crosstalk in cancer. *Cytokine Growth Factor Rev* 2010; **21**: 11–19.
43. Johnson C, Han Y, Hughart N, McCarra J, Alpini G, Meng F. Interleukin-6 and its receptor, key players in hepatobiliary inflammation and cancer. *Transl Gastrointest Cancer* 2012; **1**: 58–70.
44. Liu Y, Fuchs J, Li C, Lin J. IL-6, a risk factor for hepatocellular carcinoma: FLLL32 inhibits IL-6-induced STAT3 phosphorylation in human hepatocellular cancer cells. *Cell Cycle* 2010; **9**: 3423–3427.
45. Naugler WE, Sakurai T, Kim S, Maeda S, Kim K, Elsharkawy AM *et al.* Gender disparity in liver cancer due to sex differences in MyD88-dependent IL-6 production. *Science* 2007; **317**: 121–124.
46. Manzl C, Peintner L, Krumschnabel G, Bock F, Labi V, Drach M *et al.* PIDDosome-independent tumor suppression by Caspase-2. *Cell Death Diff* 2012; **19**: 1722–1732.
47. O'Reilly LA, Ekert P, Harvey N, Marsden V, Cullen L, Vaux DL *et al.* Caspase-2 is not required for thymocyte or neuronal apoptosis even though cleavage of caspase-2 is dependent on both Apaf-1 and caspase-9. *Cell Death Differ* 2002; **9**: 832–841.

Supplementary Information accompanies this paper on Cell Death and Differentiation website (http://www.nature.com/cdd)